

# *Isothermal crystallization of polycaprolactone/modified clay biodegradable nanocomposites*

**Matías Lanfranconi, Vera A. Alvarez & Leandro N. Ludueña**

## **Journal of Thermal Analysis and Calorimetry**

An International Forum for Thermal Studies

ISSN 1388-6150

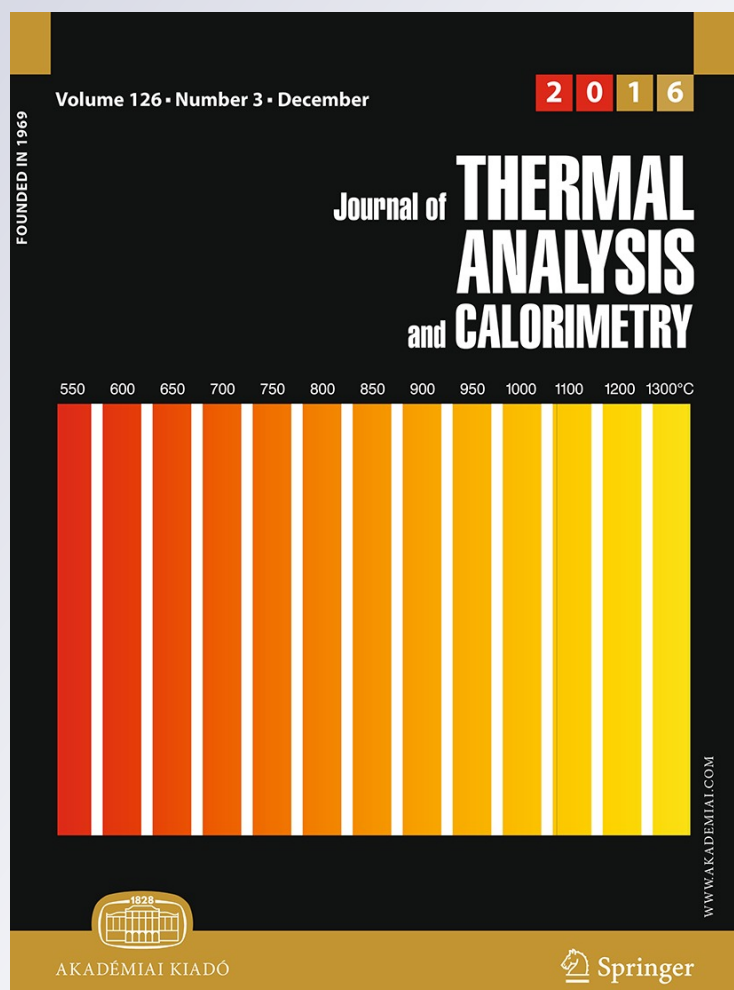
Volume 126

Number 3

J Therm Anal Calorim (2016)

126:1273-1280

DOI 10.1007/s10973-016-5734-x



**Your article is protected by copyright and all rights are held exclusively by Akadémiai Kiadó, Budapest, Hungary. This e-offprint is for personal use only and shall not be self-archived in electronic repositories. If you wish to self-archive your article, please use the accepted manuscript version for posting on your own website. You may further deposit the accepted manuscript version in any repository, provided it is only made publicly available 12 months after official publication or later and provided acknowledgement is given to the original source of publication and a link is inserted to the published article on Springer's website. The link must be accompanied by the following text: "The final publication is available at [link.springer.com](http://link.springer.com)".**

# Isothermal crystallization of polycaprolactone/modified clay biodegradable nanocomposites

Matías Lanfranconi<sup>1</sup> · Vera A. Alvarez<sup>1</sup> · Leandro N. Ludueña<sup>1</sup>

Received: 2 October 2015 / Accepted: 19 July 2016 / Published online: 2 August 2016  
© Akadémiai Kiadó, Budapest, Hungary 2016

**Abstract** In this paper, the isothermal crystallization of polycaprolactone (PCL)/modified clay nanocomposites, at several temperatures, was studied. The effects of clay type (organo-modified bentonite B-TBHP and organo-modified montmorillonite C20A) and also the clay content were analysed. Bulk crystallization was studied by differential scanning calorimetry and modelled by the Avrami equation. Special effort was made to correlate the crystallization parameters with the clay dispersion degree inside the polymer matrix. The lowest induction time and fastest overall crystallization rate were obtained with the B-TBHP nanocomposites, which showed the lowest clay dispersion degree. In contrast, C20A nanocomposites showed higher clay dispersion degree inside the PCL matrix and higher induction times and lower overall crystallization rate than B-TBHP ones, even retarding the formation of the equilibrium nucleus with critical dimensions in comparison with neat PCL.

**Keywords** Nanocomposites · Compatibility · Biodegradable polymer · Crystallization · Modelling · Bentonite

## Introduction

In the last decades, inorganic reinforcement/organic matrix nanocomposites have been analysed not only for research purposes but also for several applications [1–3], because of their unique properties. The addition of inorganic fillers (usually lower than 10 mass%) to a polymeric matrix can improve several characteristics, such as mechanical barrier and thermal properties [4–8].

The incorporation of any filler to a thermoplastic matrix not only affects its properties but also affects the crystallization behaviour. The most known effects are produced on the crystallinity degree, the crystallite size, shape and morphology of the spherulites and the crystallization kinetics of the pure matrix [9–12]. Several authors have demonstrated the nucleating and accelerating effects of clay nanoparticles by analysing different experimental parameters: the melting and crystallization temperatures ( $T_m$  and  $T_c$ ) [3, 13, 14], the crystallization rate [15, 16], the effective energy barrier [17] and the half-time for the crystallization [14, 18]. The effects of nanoparticles have been also analysed by means of theoretical models [14, 17, 18]. All crystallization parameters have a crucial role on the physical and mechanical properties of thermoplastic based materials.

Regarding polymer/clay nanocomposites, there exist controversial results related with the polymer/clay compatibility and its effect over the bulk isothermal crystallization behaviour of thermoplastic matrices. It is known that the use of different clays (un-modified and modified) is mainly associated with the improvement of their compatibility with the thermoplastic polymer matrix. Whereas some studies [11] indicate that as higher the dispersion degree is (higher matrix/clay compatibility), lower the clay nucleation effect becomes, other ones [18] correlate the

✉ Leandro N. Ludueña  
luduenanmdp@gmail.com

<sup>1</sup> Composite Materials Group (CoMP), Research Institute of Material Science and Technology (INTEMA), Engineering Faculty, National University of Mar del Plata, Solís 7575 (B7608FDQ), Mar del Plata, Argentina

nucleation effect with the contact area between polymer segments and clay surface: a higher contact area resulting from the higher clay interlayer spacing produces a greater nucleation effect.

The aim of this work was to improve the knowledge about the influence of clay morphology on the bulk isothermal crystallization process of a thermoplastic polymer matrix. The effect of clay addition, clay content and polymer/clay compatibility on the bulk isothermal crystallization process of polycaprolactone/clay nanocomposites will be analysed.

## Theoretical background

### Bulk crystallization

Table 1 shows the equations used for modelling the bulk isothermal crystallization process.

The classical Avrami equation [3, 13, 14] has been applied for the crystallization kinetics of polymer matrices under isothermal conditions and also for composites and nanocomposites [15, 16]. The Avrami exponent  $n$  depends on the nucleation mechanism and the geometry of crystal growth, and the rate constant  $k$  includes nucleation parameters as well as growth-rate parameters. The last parameter usually follows an Arrhenius-type relationship with the undercooling degree as shown in Eq. 4. The total activation energy,  $E_a$ , consists of the transport activation energy ( $E^*$ ) and the nucleation activation energy ( $E_f$ ).  $E^*$

refers to the activation energy required to transport molecular segments across the phase boundary to the crystallization surface, and  $E_f$  is the free energy of formation of the critical size crystal nuclei at  $T_c$  [19].

During the isothermal crystallization carried out in DSC, the crystallization heat, obtained by measuring the area under the exothermic peak [17], can be transformed into the relative degree of crystallinity,  $\alpha$ , by dividing the heat developed at each crystallization time  $t$  ( $\Delta H_t$ ) by the total area under the exothermic peak.

## Experimental

### Materials

PCL (Mn 80000, Sigma-Aldrich) was used as matrix. Cloisite 20A (C20A, Southern Clay Products) and bentonite (Minarmco S.A.) were used as fillers. The bentonite was organo-modified with tributylhexadecylphosphonium bromide (Sigma-Aldrich).

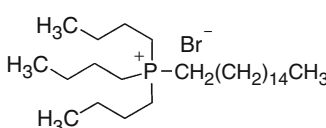
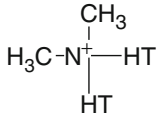
### Modification of bentonite with tributylhexadecylphosphonium bromide [20]

2.5 g of clay was dispersed in 100 mL of deionized water. Then, the aqueous solution of TBHP (3.CEC) of the corresponding concentration was added. The mixture was stirred for 4 h at 70 °C. After that, the suspension was filtered through a Buchner Funnel and washed with

**Table 1** Equations used for the modelling of bulk isothermal crystallization process

Isothermal crystallization		
Relative degree of crystallinity	$\alpha = \frac{\int_0^t \frac{dH_t}{dt} dt}{\int_0^\infty \frac{dH_t}{dt} dt} = \frac{\Delta H_t}{\Delta H_0} \quad (1)$	$\Delta H_t$ : heat generated at time $t$ [14] $\Delta H_0$ : total heat generated up to the complete crystallization
Rate constant	$\frac{1}{t_{1/2}} = \text{OCR} \quad (2)$	$t_{1/2}$ : half crystallization time (time at which the relative degree of crystallinity approaches to 0.5) OCR: overall crystallization rate
Hoffman–Weeks method	$T_m^0$ is obtained from the interception of $T_m = f(T_c)$ at $T_m = T_c$	$T_m$ : meeting temperature [19] $T_c$ : crystallization temperature
Avrami's model	$\alpha = 1 - \exp(-k \cdot t^n) \quad (3)$	$k$ : Avrami's rate constant (containing the nucleation and the growth parameters) [20] $n$ : Avrami exponent (depends on the mechanism of nucleation and on the form of crystal growth)
Rate constant	$k = k_0 \cdot \exp\left(-\frac{E_a}{R \cdot (T_m^0 - T_c)}\right) \quad (4)$	$k_0$ : pre-exponential factor [21] $R$ : universal gas constant $E_a$ : total activation energy $T_m^0$ : theoretical melting point $T_c$ : crystallization temperature. $T_m^0 - T_c$ = undercooling degree

**Table 2** Characteristics of clays used as fillers of PCL

Clay	Organic modifier <sup>a</sup>	Absorbed water 24 h at 90 % RH (%)	$d_{001}/\text{nm}$	OC/%	$T_p/^\circ\text{C}$
B-TBHP		2.73	2.51	29	388.7
C20A		3.72	2.42	41	303.1

<sup>a</sup> HT hydrogenated tallow (65 % C18; 30 % C16; 5 % C14)

deionized water until free of bromide. The organo-clays were dried with a freeze dry system. The organo-modified bentonite was named B-TBHP.

The characteristics of both used organo-clays are included in Table 2.

#### Preparation of nanocomposites

Nanocomposites with 0.0, 2.5, 5.0 and 7.5 mass% of each clay were prepared by melt intercalation in a Brabender type mixer at 100 °C and 150 rpm for 10 min. Then, films with a thickness of 0.3–0.5 mm were prepared by compression moulding in a hydraulic press for 10 min at 100 °C. The nanocomposite films were identified by a number corresponding to the mass% of clay followed by the name of the nanoclay, i.e.: 2.5B-TBHP is the nanocomposite based on PCL with 2.5 mass% of B-TBHP.

#### Methods

X-ray diffractometry (XRD) of clay powders and nanocomposites was performed using a PANalytical X'Pert PRO diffractometer equipped with  $\text{CuK}\alpha$  radiation ( $\lambda = 1.5406 \text{ \AA}$ ) operating at 40 kV and 40 mA, at a scanning speed of  $1^\circ \text{ min}^{-1}$ .

Thermogravimetric analysis (TG) was performed in a TA Auto-MTGA Q500 Hi-Res from 30 to 900 °C at  $10^\circ \text{C min}^{-1}$  under air atmosphere. The organic content (OC) of the neat clays was calculated from the mass loss between 200 and 500 °C. The temperature for the maximum thermal degradation rate of the organo-modifiers ( $T_p$ ) was calculated by derivative thermogravimetric analysis (DTG) from the position of the peak between 200 and 500 °C. Both parameters were reported in Table 2. Tests in nitrogen atmosphere were done to calculate the clay content inside the nanocomposites. These values were calculated from the residual mass of the composites at 900 °C correcting for the residual mass of the neat matrix and for the mass loss of the neat clays at the same temperature. The mass loss of the neat clays at 900 °C is mainly composed

of water and/or organic content. These calculations were carried out assuming that thermal degradation of the clay organo-modifiers did not take place during the intercalation process.

Bulk crystallization process was measured by means of a MDSC Q2000 RCS90, (Modulated Differential Scanning Calorimeter) TA Instruments, under nitrogen atmosphere. The following steps were applied to each sample:

1. Heating from room temperature to 100 °C at  $10^\circ \text{C min}^{-1}$ .
2. Melting at 100 °C for 10 min.
3. Cooling to the crystallization temperature (between 36 and 42 °C) at  $40^\circ \text{C min}^{-1}$ .
4. Holding at the crystallization temperature 30 min to allow complete crystallization.
5. Heating from the crystallization temperature to 100 °C at  $10^\circ \text{C min}^{-1}$  to melt formed crystals at the crystallization temperature and to find the melting temperature of each material.

The degree of crystallinity was calculated from the following equation [14]:

$$X_{\text{cr}}(\%) = \frac{\Delta H_f}{w_{\text{PCL}} \times \Delta H_{100}} \times 100 \% \quad (5)$$

where  $\Delta H_f$  is the experimental heat of fusion,  $w_{\text{PCL}}$  is mass fraction of the matrix and  $\Delta H_{100}$  is the heat of fusion of the polycaprolactone 100 % crystalline. The value was obtained from the literature and it was  $136.1 \text{ J g}^{-1}$  [14].

#### Results and discussion

The morphology of the materials studied in this work was analysed by X-ray diffractometry. The basal spacing, also known as interlayer distance ( $d_{001}$ ), of the neat clays and inside the nanocomposites was calculated from the  $2\theta$  values of the corresponding peaks in the X-ray curves using the Bragg's equation. The  $d_{001}$  value of the neat clays and inside the nanocomposites is reported in Table 2 and

**Table 3** Interlayer distance ( $d_{001}$ ), heat of melting ( $\Delta H_m$ ), degree of crystallinity ( $X_{cr}$ ) and theoretical melting temperature ( $T_m^0$ ) for the matrix and nanocomposites

Material	$d_{001}/\text{nm}$	$\Delta H_m/\text{J g}^{-1}$	$X_{cr}/\%$	$T_m^0/^\circ\text{C}$	Material	$d_{001}/\text{nm}$	$\Delta H_m/\text{J g}^{-1}$	$X_{cr}/\%$	$T_m^0/^\circ\text{C}$
PCL	–	83.6	61.5	64	PCL	–	83.6	61.5	64
2.5C20A	3.51	84.2	63.5	64	2.5B-TBHP	3.29	87.2	63.5	64
5.0C20A	3.32	83.1	64.3	64	5.0B-TBHP	3.25	84.0	64.3	64
7.5C20A	3.55	81.4	64.7	64	7.5B-TBHP	3.45	80.1	64.7	64

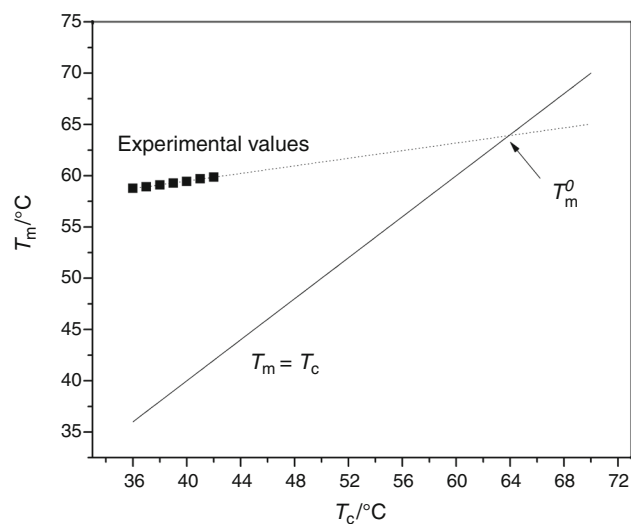
Table 3, respectively. We found larger interlayer distance for the PCL/C20A nanocomposites, compared with that of the PCL/B-TBHP samples at the same clay content. This result indicates higher intercalation degree of the PCL chains into the C20A platelets. It also confirms the improved clay dispersion degree of C20A inside the PCL matrix [21]. Analysing the effect of clay content on the morphology of the nanocomposites, we found that the interlayer distance of C20A inside the PCL matrix decreases 5 % from 2.5 to 5.0 mass% and then increase 6 % from 5.0 to 7.5 mass%, suggesting slight agglomeration at 5 mass%. The same trend was found for the B-TBHP nanocomposites [22].

Table 3 summarized the heat of melting ( $\Delta H_m$ ), the degree of crystallinity ( $X_{cr}$ ) and the theoretical melting temperature ( $T_m^0$ ) for the matrix and nanocomposites. Figure 1 shows the experimental curves of melting temperature ( $T_m$ ) as a function of crystallization temperature ( $T_c$ ) and the curve at  $T_m = T_c$  that were used for the calculation of  $T_m^0$  for the neat PCL matrix following the Hoffman–Weeks method. Similar curves were obtained for the nanocomposites. The degree of crystallinity remained almost constant, and the theoretical melting temperature was in the range of  $64 \pm 0.5$  °C after clay incorporation. Similar trend was found by Kelnar et al. [23] in the case of nanocomposites based on polycaprolactone with 3 mass% of Cloisite 15A and Ludueña et al. [24] for PCL/montmorillonite nanocomposites. On the other hand, Olewnik et al. [25] showed increased crystallinity of polyethylene after incorporation of n-heptaquinolinium modified montmorillonite, but in this case, conventional microcomposites were obtained due to a non-effective polymer/clay compatibilization.

### Induction time and overall crystallization rate

Figure 2a, b shows the relative degree of crystallinity ( $\alpha$ ) as a function of time ( $t$ ) for PCL and the nanocomposite 2.5B-TBHP at several undercooling degrees ( $\Delta T = T_m^0 - T_c$ ). Similar curves were observed for all nanocomposites.

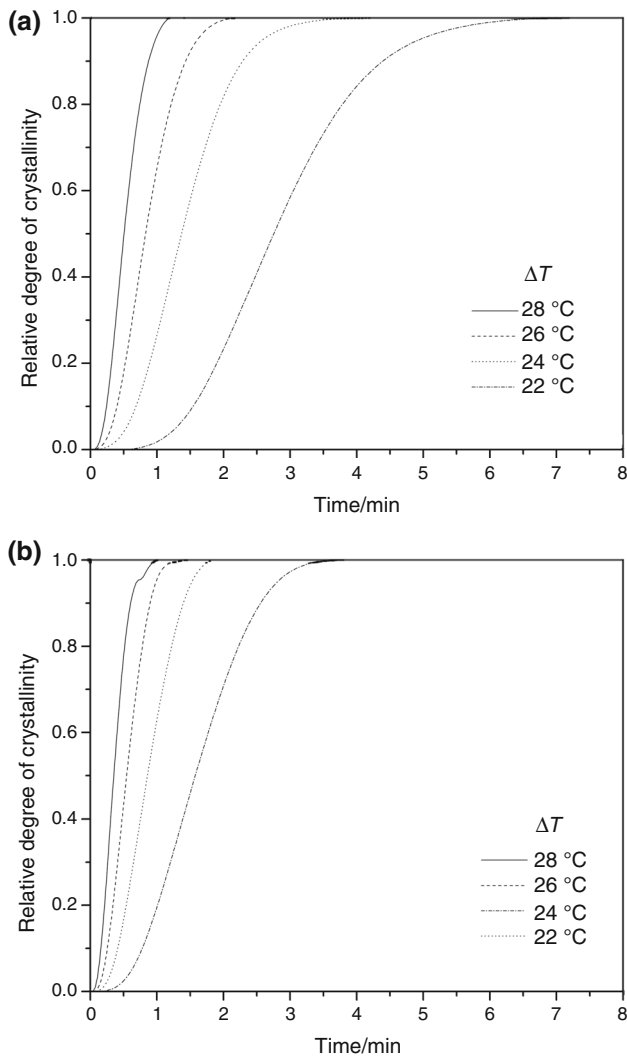
It can be seen a shift of the curves towards lower times and an increment of the slope of their linear portion as a

**Fig. 1** Determination of  $T_m^0$  for PCL matrix following the Hoffman–Weeks method

function of the undercooling degree, implying that a higher undercooling degree leads to a higher crystallization rate.

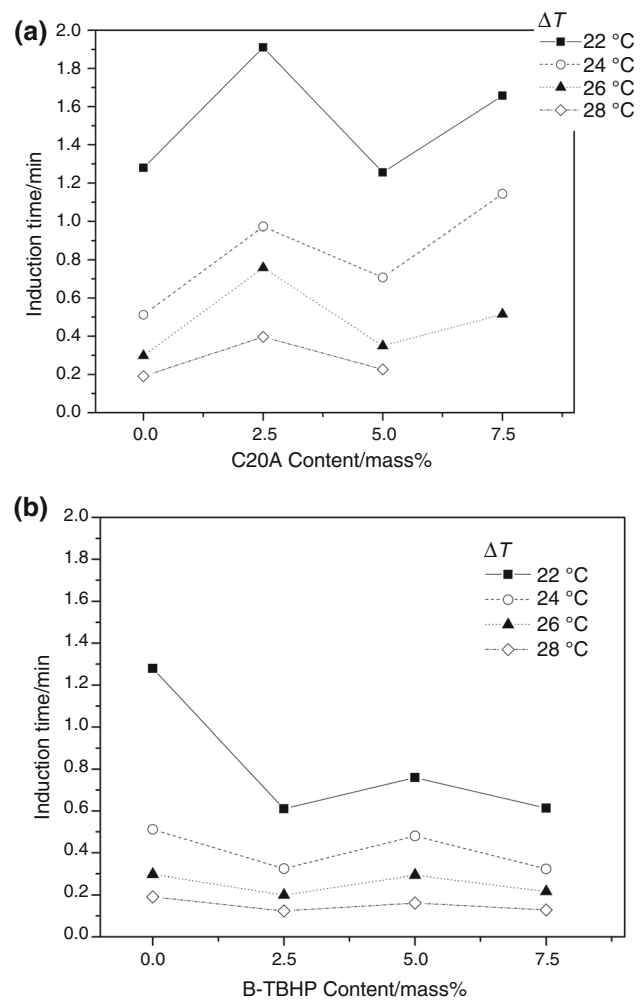
An approximation of the crystallization rate can be made by the overall crystallization rate ( $1/t_{1/2}$ ), where  $t_{1/2}$  (half crystallization time) is the time at which the relative degree of crystallinity ( $\alpha$ ) approach the value of 0.5. This parameter is proportional to both the primary nucleation rate and the crystal/spherulite growth so induction time ( $t_{ind}$ ) has to be also taken into account when  $t_{1/2}$  is analysed [26]. Induction time ( $t_{ind}$ ) is the time needed for the formation of the equilibrium nucleus with critical dimensions at a given undercooling degree.

Figure 3a, b show the induction time as a function of clay content. In all cases, the induction time decreases as a function of undercooling degree. This result was expected since the undercooling degree is the driving force for the formation of the equilibrium nucleus with critical dimensions. Same trend was found in a previous work [24] for PCL reinforced with two clays: natural montmorillonite (MMT) and a commercial organo-modified montmorillonite Cloisite 30B (C30B). In that work, we also found that the nanocomposite with the lowest clay dispersion degree leads to the lowest induction time comparing at the



**Fig. 2** Relative degree of crystallinity ( $\alpha$ ) as a function of time ( $t$ ) for: **a** PCL; **b** 2.5B-TBHP

same clay content and undercooling degree. Krikorian et al. [11] obtained the same result after studying the crystallization behaviour of Polylactic acid (PLLA)/MMT and PLLA/C30B nanocomposites. In addition, both works showed that MMT and C30B clays act as nucleation agents lowering the induction time in comparison with that of the neat polymer matrix. The same trend was obtained in this work; lower induction time was obtained for the B-TBHP nanocomposites, which showed the lowest clay dispersion degree. On the other hand, C20A showed higher clay dispersion degree inside the PCL matrix and higher induction times than B-TBHP ones but did not act as nucleation agent. In fact, C20A acted retarding the formation of the equilibrium nucleus with critical dimensions in comparison with neat PCL. This result may be expected if the dispersion degree of C20A inside PCL is even higher than that of



**Fig. 3** Induction time as a function of clay content at several undercooling degrees: **a** C20A nanocomposites; **b** B-TBHP nanocomposites

C30B, which was demonstrated in previous works [27, 28] by X-ray diffractometry, melt rheology and electron transmission microscopy. The anti-nucleating effect was also observed by Díaz et al. [29] for polylactic acid/Cloisite 25A nanocomposites with exfoliated morphology. Analysing the effect of clay content, we can observe that 5 mass% of C20A clearly decreases the induction time in comparison with 2.5C20A and 7.5C20A nanocomposites. In the case of the B-TBHP nanocomposites, the opposite trend was observed, the induction time slightly increases at 5.0 mass% and then decreases for 7.5 mass%.

Figure 4a, b shows the overall crystallization rate (OCR) as a function of clay content. OCR followed the same trends as induction time, which is expected because OCR is proportional to both the primary nucleation rate and the crystal/spherulite growth so induction time has to be also taken into account when OCR is analysed. OCR was higher

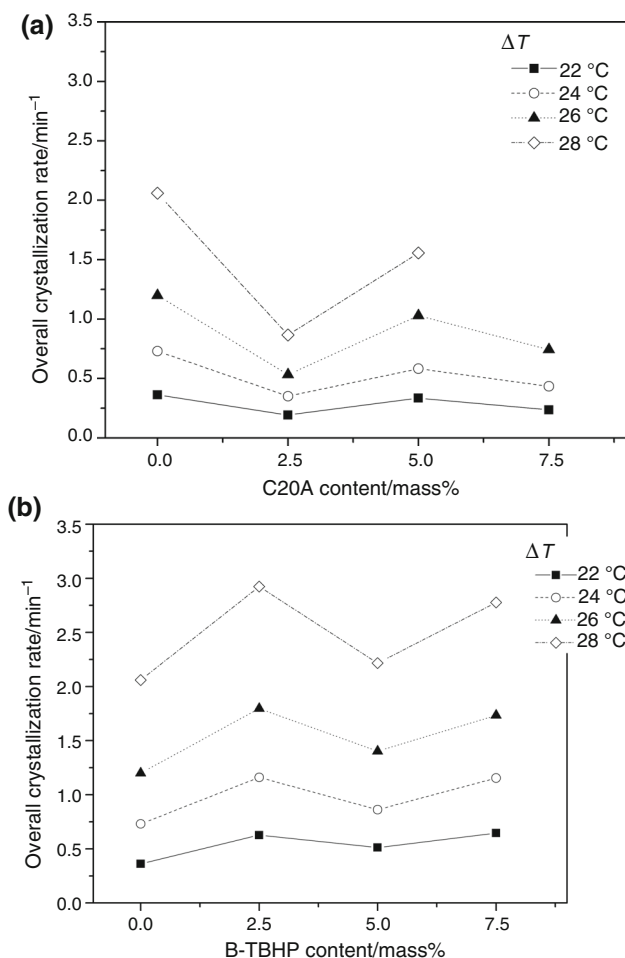


**Fig. 4** Overall crystallization rate as a function of clay content at several undercooling degrees: **a** C20A nanocomposites; **b** B-TBHP nanocomposites

as a function of undercooling degree and lower as a function of clay dispersion degree. Krikorian et al. [11] found a similar tendency in the case of poly(L-lactic acid)/MMT-C30B nanocomposites, establishing the hypothesis that when the clay/polymer compatibility is improved, dispersed clay platelets may hinder the chain-folding mechanism for local poly(L-lactic acid) crystallization.

In conclusion, we can recognize two mechanisms that have opposite effects in the isothermal crystallization process of polymer/clay nanocomposites: (1) clays acting as nucleation agents decreasing  $t_{ind}$  and increasing OCR and (2) clays hindering the chains folding mechanism for local polymer crystallization increasing  $t_{ind}$  and decreasing OCR. The same hypothesis was previously stated by Gupta et al. [30] for non-isothermal crystallization of polyurethane/clay nanocomposites but they did not relate it with the clay dispersion degree inside the polymer matrix. In our case, we demonstrated that both

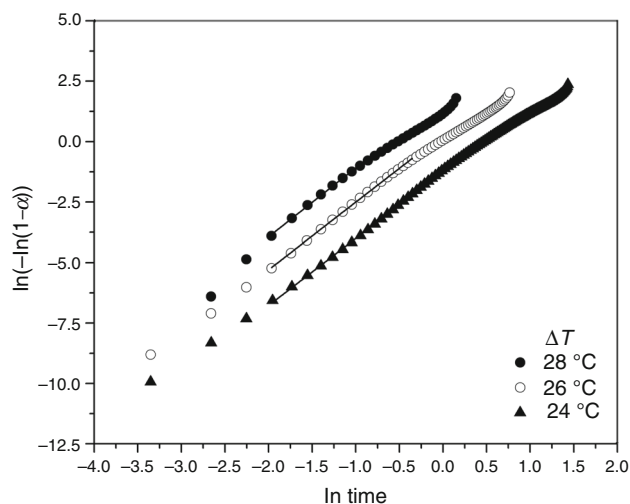


**Fig. 5** Calculation of the Avrami exponent ( $n$ ) and the rate constant ( $k$ ) by linear regression for the neat PCL

phenomena can be present in all polymer/clay nanocomposites but one of them will dominate the crystallization process depending on the clay dispersion degree of the nanocomposite. The dominant effect may be activated at a critical clay dispersion degree for a certain polymer/clay system. In cases of low clay dispersion degree at which clay acting as nucleation agent is the dominant mechanism, further agglomeration would reduce the number of nucleation sites retarding nucleation time and decreasing OCR. This may be the situation for B-TBHP nanocomposites for which  $t_{ind}$  decreases and OCR increases for 2.5B-TBHP in comparison with neat PCL, then slight agglomeration takes places at 5.0B-TBHP slightly increasing  $t_{ind}$  (but still lower than neat matrix) and decreasing OCR and finally the clay dispersion degree is improved for 7.5B-TBHP and the  $t_{ind}$  and OCR return to values close to those of 2.5B-TBHP. On the other hand, higher clay dispersion degrees at which clays hindering the chains folding mechanism for local polymer crystallization are the dominant phenomena, and agglomeration reduces the probability of building rigid clays structures promoted by edge-edge and face-edge clay platelet interactions weakening the retarding effect on induction time and increasing OCR. This may be the situation for C20A nanocomposites for which the clays act retarding the nucleation and the overall crystallization rate for 2.5C20A in comparison with the neat PCL, then agglomeration takes place at 5.0C20A accelerating the isothermal crystallization process (but still retarded in comparison with the neat PCL) and then the clay dispersion degree is improved for 7.5C20A and the retarding effect becomes stronger again.



**Table 4** Parameters obtained from Avrami's modelling

Material	Average $n$	$k$ at $\Delta T = 26$ °C/s <sup>-<math>n</math></sup>	$k_0/s^{-n}$	$E_a/kJ\ mol^{-1}$	Material	Average $n$	$k$ at $\Delta T = 26$ °C/s <sup>-<math>n</math></sup>	$k_0/s^{-n}$	$E_a$ (kJ mol <sup>-1</sup> )
PCL	2.8	1.34	$3.26 \times 10^8$	4.2	PCL	2.8	1.34	$3.26 \times 10^8$	4.2
2.5C20A	2.5	0.13	$1.34 \times 10^5$	2.9	2.5B-TBHP	2.8	4.85	$1.24 \times 10^5$	2.2
5.0C20A	2.7	0.76	$1.59 \times 10^7$	3.7	5.0B-TBHP	2.7	1.88	$6.04 \times 10^6$	3.2
7.5C20A	2.7	0.31	$4.73 \times 10^2$	1.6	7.5B-TBHP	2.4	3.22	$2.81 \times 10^4$	2.0

### Isothermal bulk crystallization modelling

The Avrami exponent  $n$  and rate constant  $k$  (Eq. 4) were calculated with a linear regression method as shown in Fig. 5 for the neat PCL. Same procedure was used for the nanocomposites. Table 3 summarizes the obtained values. In the case of the rate constant, only the values at  $\Delta T = 26$  °C were shown for the sake of simplicity. Same trend was observed at all undercooling degrees analysed. Values are summarized in Table 4.

The average  $n$  value for the matrix and nanocomposites was between 2.5 and 3 for all materials. The  $n$  value slightly decreased after clay incorporation. Similar trend was obtained by Chen et al. [31] for poly(butylene succinate) in the presence of organically modified clay at different loadings. In the ideal case,  $n = 3$  indicates spherical growth, whereas  $n = 2$  indicates circular disc-shaped growth [32].

In all cases,  $k$  increased as a function of the undercooling degree because the driving force became higher. In the case of C20A,  $k$  decreases in comparison with the neat matrix. The retarding effect is less notorious for the 5.0C20A nanocomposite. Adding B-TBHP to PCL increases the  $k$  values for all clay contents analysed in comparison with the neat matrix. This result is also in accordance with OCR and morphology analysis and with the hypothesis of higher crystallization rate for lower clay dispersion degree. On the other hand,  $k$  as a function of clay B-TBHP content showed the opposite trend than C20A nanocomposites. Even when all  $k$  values of B-TBHP nanocomposites are higher than that of the neat matrix,  $k$  decreases for the 5.0B-TBHP and then increases again for 7.5B-TBHP. For C20A nanocomposites,  $k$  increases for the 5.0C20A and then decreases again for 7.5C20A. These results are in accordance with the experimental induction time and OCR values for both nanocomposites as a function of the clay content, which supports the conclusions of that section.

The rate constant ( $k$ ) can be fitted by an Arrhenius-type equation as shown in Eq. 5. A typical linear regression method was used to fit the double logarithmic plot of rate constant values ( $k$ ) as a function of undercooling degree

calculating the pre-exponential factor  $k_0$  and the total activation energy  $E_a$ . Table 4 shows the obtained values. The B-TBHP nanocomposites showed lower  $E_a$  than the C20A ones at the same clay content. This result is in accordance with the OCR analysis which can be correlated with the differences in the clay dispersion degree of the nanocomposites. It can be also observed that the  $E_a$  values of the C20A nanocomposites were lower than that of the neat PCL matrix. It was previously demonstrated that C20A clay retards the bulk crystallization process of PCL, so higher  $E_a$  values for the C20A nanocomposites would be expected.

### Conclusions

Nanocomposites with 2.5, 5.0 and 7.5 mass% of two organo-modified clays were prepared by melt intercalation. Clay morphology was studied by X-ray diffractometry. For both clays, agglomeration at 5 mass% of clay was found and then improved again at 7.5 mass%. It was shown that the presence of the clay affects the bulk isothermal crystallization process of PCL/clay nanocomposites. The induction time and the overall crystallization rate were strictly dependent on the clay dispersion degree inside the nanocomposites. The nanocomposites with lower clay dispersion degree (PCL/B-TBHP) showed shorter induction times, faster overall crystallization rates and higher Avrami's rate constants. The agglomeration found for the 5 mass% of clay became this effect weaker. On the other hand, the nanocomposites with improved clay dispersion degree (PCL/C20A), retarded the induction time and decreased the overall crystallization rate in comparison with the neat matrix. This effect was also weaker for the 5 mass% nanocomposite for which agglomeration was observed. The theoretical parameters from the Avrami's modelling showed the same trends than the experimental ones as a function of clay dispersion degree.

**Acknowledgements** This work was supported by the National Agency of Science and Technology (ANPCyT) [Fonarsac FSNano004] and the National University of Mar del Plata (UNMdP) [15G327].

## References

1. Xu W, Ge M, He P. Nonisothermal crystallization kinetics of polyoxymethylene/montmorillonite nanocomposite. *J Appl Polym Sci.* 2001;82(9):2281–9.
2. Ke Y, Long C, Qi Z. Crystallization, properties, and crystal and nanoscale morphology of PET–clay nanocomposites. *J Appl Polym Sci.* 1999;71(7):1139–46.
3. Liu X, Wu Q. PP/clay nanocomposites prepared by grafting–melt intercalation. *Polymer.* 2001;42(25):10013–9.
4. Alexandre M, Dubois P. Polymer-layered silicate nanocomposites: preparation, properties and uses of a new class of materials. *Mat Sci Eng R Rep.* 2000;28(1):1–63.
5. Messersmith PB, Giannelis EP. Synthesis and barrier properties of poly ( $\epsilon$ -caprolactone)-layered silicate nanocomposites. *J Polym Sci Part A Polym Chem.* 1995;33(7):1047–57.
6. Kojima Y, Usuki A, Kawasumi M, Okada A, Fukushima Y, Kurauchi T, et al. Mechanical properties of nylon 6-clay hybrid. *J Mat Res.* 1993;8(05):1185–9.
7. Gilman JW, Jackson CL, Morgan AB, Harris R Jr, Manias E, Giannelis EP, et al. Flammability properties of polymer-layered-silicate nanocomposites. Polypropylene and polystyrene nanocomposites. *Chem Mat.* 2000;12(7):1866–73.
8. Gorrasi G, Tortora M, Vittoria V, Pollet E, Lepoittevin B, Alexandre M, et al. Vapor barrier properties of polycaprolactone montmorillonite nanocomposites: effect of clay dispersion. *Polymer.* 2003;44(8):2271–9.
9. Di Maio E, Iannace S, Sorrentino L, Nicolais L. Isothermal crystallization in PCL/clay nanocomposites investigated with thermal and rheometric methods. *Polymer.* 2004;45(26):8893–900.
10. Homminga D, Goderis B, Dolbnya I, Groeninckx G. Crystallization behavior of polymer/montmorillonite nanocomposites. Part II. Intercalated poly ( $\epsilon$ -caprolactone)/montmorillonite nanocomposites. *Polymer.* 2006;47(5):1620–9.
11. Krikorian V, Pochan DJ. Unusual crystallization behavior of organoclay reinforced poly (L-lactic acid) nanocomposites. *Macromolecules.* 2004;37(17):6480–91.
12. Kennedy M, Turturro G, Brown G, St-Pierre L. Silica retards radial growth of spherulites in isotactic polystyrene. *Nature.* 1980;287:316–17.
13. Jain S, Goossens H, van Duin M, Lemstra P. Effect of in situ prepared silica nano-particles on non-isothermal crystallization of polypropylene. *Polymer.* 2005;46(20):8805–18.
14. Yuan Q, Awate S, Misra R. Nonisothermal crystallization behavior of polypropylene–clay nanocomposites. *Eur Polym J.* 2006;42(9):1994–2003.
15. Papageorgiou GZ, Achilias DS, Bikiaris DN. Crystallization kinetics of biodegradable poly (butylene succinate) under isothermal and non-isothermal conditions. *Macromol Chem Phys.* 2007;208(12):1250–64.
16. Medellín-Rodríguez F, Mata-Padilla J, Hsiao B, Waldo-Mendoza M, Ramirez-Vargas E, Sanchez-Valdes S. The effect of nanoclays on the nucleation, crystallization, and melting mechanisms of isotactic polypropylene. *Polym Eng Sci.* 2007;47(11):1889.
17. Xu W, Ge M, He P. Nonisothermal crystallization kinetics of polypropylene/montmorillonite nanocomposites. *J Polym Sci Part B Polym Phys.* 2002;40(5):408–14.
18. Xu W, Liang G, Zhai H, Tang S, Hang G, Pan W-P. Preparation and crystallization behaviour of PP/PP-g-MAH/Org-MMT nanocomposite. *Eur Polym J.* 2003;39(7):1467–74.
19. Birgersson E, Li H, Wu S. Transient analysis of temperature-sensitive neutral hydrogels. *J Mech Phys Sol.* 2008;56(2):444–66.
20. Ollier R, Vázquez A, Alvarez V. Biodegradable nanocomposites based on modified bentonite and polycaprolactone. In: *Advances in nanotechnology.* New York: Nova Publishers; 2011. p. 281–301.
21. Wagener R, Reisinger TJ. A rheological method to compare the degree of exfoliation of nanocomposites. *Polymer.* 2003;44(24):7513–8.
22. Ollier R, Lanfranconi M, Ludueña L, Alvarez V (eds.) Preparation and characterization of PCL/modified-clay biodegradable nanocomposites Euporean polymer conference EPF 2013 2013 2013; Pisa.
23. Kelnar I, Kratochvíl J, Kaprálková L. Crystallization and thermal properties of melt-drawn PCL/PLA microfibrillar composites. *J Therm Anal Calorim.* 2016;124:799–805.
24. Ludueña LN, Vazquez A, Alvarez VA. Crystallization of polycaprolactone–clay nanocomposites. *J Appl Polym Sci.* 2008;109(5):3148–56.
25. Olewnik E, Garman K. Thermal properties of nanocomposites based on polyethylene and n-heptaquinolinum modified montmorillonite. *J Therm Anal Calorim.* 2012;110:479–84.
26. Jimenez G, Ogata N, Kawai H, Ogihara T. Structure and thermal/mechanical properties of poly ( $\epsilon$ -caprolactone)-clay blend. *J Appl Polym Sci.* 1997;64(11):2211–20.
27. Luduena L, Kenny J, Vázquez A, Alvarez V. Effect of clay organic modifier on the final performance of PCL/clay nanocomposites. *Mat Sci Eng A.* 2011;529:215–23.
28. Ludueña L, Vázquez A, Alvarez V. Effect of the type of clay organo-modifier on the morphology, thermal/mechanical/impact/barrier properties and biodegradation in soil of polycaprolactone/clay nanocomposites. *J Appl Polym Sci.* 2013;128(5):2648–57.
29. Díaz A, Franco L, Casas M, del Valle L, Aymamí J, Olmo C, Puiggalí J. Preparation of micro-molded exfoliated clay nanocomposites by means of ultrasonic technology. *J Polym Res.* 2014;21:584.
30. Gupta Y, Abbas S, Sharma R, Setua D. Crystallization kinetics of polyurethane nanocomposites. *J Therm Anal Calorim.* 2015;119:1393–405.
31. Chen J, Xu J, Xu H, Li Z, Zhong G, Lei J. The crystallization behavior of biodegradable poly(butylene succinate) in the presence of organically modified clay with a wide range of loadings. *Chin J Polym Sci.* 2015;33(4):576–86.
32. Desio GP, Rebenfeld L. Crystallization of fiber-reinforced poly (phenylene sulfide) composites II Modeling the crystallization kinetics. *J Appl Polym Sci.* 1992;45(11):2005–20.